JACS
JOURNAL OF THE AMERICAN CHEMICAL SOCIETY
Article
pubs.acs.org/JACS

# Benzothienobenzothiophene-Based Molecular Conductors: High Conductivity, Large Thermoelectric Power Factor, and One-Dimensional Instability

Yasuhiro Kiyota,[†] Tomofumi Kadoya,[*,†,⊥] Kaoru Yamamoto,[*,‡] Kodai Iijima,[†] Toshiki Higashino,[†,#] Tadashi Kawamoto,[†] Kazuo Takimiya,[§] and Takehiko Mori[*,†,∥]

[†]Department of Organic and Polymeric Materials, Tokyo Institute of Technology, O-okayama 2-12-1, Meguro-ku, Tokyo 152-8552, Japan

[‡]Department of Applied Physics, Okayama University of Science, Ridaicho 1-1, Okayama 700-0005, Japan

[§]Emergent Molecular Function Research Group, RIKEN Center for Emergent Matter Science (CEMS), Wako, Saitama 351-0198, Japan

[∥]ACT-C, JST, Honcho, Kawaguchi, Saitama 332-0012, Japan

Supporting Information

**ABSTRACT:** On the basis of an excellent transistor material, [1]benzothieno[3,2-*b*][1]benzothiophene (BTBT), a series of highly conductive organic metals with the composition of $(BTBT)_2XF_6$ (X = P, As, Sb, and Ta) are prepared and the structural and physical properties are investigated. The room-temperature conductivity amounts to 4100 S cm$^{-1}$ in the $AsF_6$ salt, corresponding to the drift mobility of 16 cm$^2$ V$^{-1}$ s$^{-1}$. Owing to the high conductivity, this salt shows a thermoelectric power factor of 55−88 $\mu$W K$^{-2}$ m$^{-1}$, which is a large value when this compound is regarded as an organic thermoelectric material. The thermoelectric power and the reflectance spectrum indicate a large bandwidth of 1.4 eV. These salts exhibit an abrupt resistivity jump under 200 K, which turns to an insulating state below 60 K. The paramagnetic spin susceptibility, and the Raman and the IR spectra suggest $4k_F$ charge-density waves as an origin of the low-temperature insulating state.


## 1. INTRODUCTION

[1]Benzothieno[3,2-*b*][1]benzothiophene (BTBT, Chart 1) derivatives are excellent organic field-effect transistor materials which show high performance and long-term stability.[1−4] Recently, the solution-processed highly crystalline transistors have realized very high mobilities of more than 30 cm$^2$ V$^{-1}$ s$^{-1}$.[5−7] In contrast to the field-effect transistors, chemical doping is another way to generate charge carriers in organic compounds. For example, a charge-transfer (CT) complex, tetrathiafulvalene:tetracyanoquinodimethane (TTF)(TCNQ), shows a room-temperature conductivity of $\sigma$ = 600 S cm$^{-1}$.[8] Formation of a CT complex is sometimes utilized in organic transistors; for example, TCNQ doping near the source and drain contacts is a usual way to reduce the contact resistance.[9] Alternatively, we can replace the whole metal contact with a conducting CT complex, and the use of (TTF)(TCNQ) contact is a convenient way to achieve low contact resistance.[10] We have further investigated "self-contact" organic transistors, in which the electrode parts are constructed by chemical doping to the active layer.[11] Therefore, it is important to investigate CT complexes of BTBT derivatives. Dialkyl-BTBT forms mix-stacked CT complexes with TCNQ derivatives. The resulting complexes are not very conducting but afford air-stable n-channel transistors.[12] We have found that unsubstituted BTBT forms a metallic CT complex with the composition of $(BTBT)_2PF_6$, and this complex shows very high room-temperature conductivity of 1500 S cm$^{-1}$.[13] Since each molecule has an average 0.5+ charge, the drift mobility is estimated to be 5.7 cm$^2$ V$^{-1}$ s$^{-1}$. Many metallic organic conductors undergo metal−insulator transitions at low temperatures, but the nature of the insulating states has a vast variety due to the electron correlation.[14] It is therefore important to identify the nature of the insulating state in order to understand the character of the donor molecule.

**Chart 1. Molecular Structures of the Representative Organic Molecules**

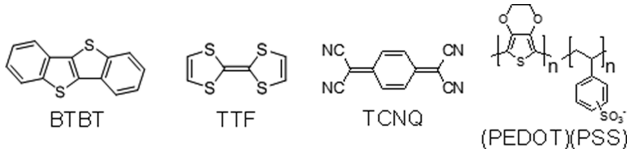


**Received:** February 2, 2016
**Published:** March 4, 2016




DOI: 10.1021/jacs.6b01213
J. Am. Chem. Soc. 2016, 138, 3920−3925

Table 1. Crystallographic Data and Calculated Transfer Integrals of $(BTBT)_2XF_6$ (X = P, As, Sb, and Ta)

| | $(BTBT)_2PF_6$[a] | $(BTBT)_2AsF_6$ | $(BTBT)_2SbF_6$ | $(BTBT)_2TaF_6$ |
|---|---|---|---|---|
| formula | $C_{28}H_{16}F_6PS_4$ | $C_{28}H_{16}F_6AsS_4$ | $C_{28}H_{16}F_6SbS_4$ | $C_{28}H_{16}F_6TaS_4$ |
| $M$ | 625.69 | 669.64 | 716.48 | 775.67 |
| crystal system | Tetragonal | Tetragonal | Tetragonal | Tetragonal |
| space group | $P\text{-}42_1c$ | $P\text{-}42_1c$ | $P\text{-}42_1c$ | $P\text{-}42_1c$ |
| $a$ (Å) | 13.4896(14) | 13.5835(13) | 13.7406(18) | 13.763(3) |
| $c$ (Å) | 6.7343(18) | 6.737(3) | 6.744(3) | 6.746(4) |
| $V$ (Å$^3$) | 1225.4(4) | 1243.1(6) | 1273.3(5) | 1277.9(8) |
| GOF | 0.854 | 1.049 | 1.275 | 1.019 |
| Unique reflections | 1120 | 1136 | 1164 | 1169 |
| Reflections [$I > 2\sigma(I)$] | 718 | 677 | 729 | 707 |
| $R_1$[b] | 0.0392 | 0.0467 | 0.0404 | 0.0478 |
| $wR_2$[c] | 0.1368 | 0.1245 | 0.0737 | 0.1459 |
| $t_c$ (meV) | 87 | 87 | 89 | 85 |
| $t_{p1}$ (meV) | 1.4 | 1.3 | 1.1 | 1.1 |
| $t_{p2}$ (meV) | 0.12 | −0.05 | −0.24 | −0.20 |
| $T$ (K) | 298 | 298 | 298 | 298 |

[a]Ref 13. [b]$I > 2\sigma(I)$. [c]All reflections.

On the other hand, recently, considerable attention has been devoted to thermoelectric materials, which directly transform heat flow to electrical energy.[15,16] Organic thermoelectric materials have great potential for flexible, low-cost, and large-area thermoelectric applications around ambient temperature. A variety of conducting polymers have been investigated from this viewpoint.[17−21] Efficiency of thermoelectric materials is represented by the figure of merit $ZT = S^2\sigma T/\kappa$, where $T$ is the temperature, $S$ is the Seebeck coefficient, and $\kappa$ is the thermal conductivity. Small $\kappa$ around 0.2 W K$^{-1}$ m$^{-1}$ is a merit of organic materials in comparison with large $\kappa$ of 10−100 W K$^{-1}$ m$^{-1}$ in inorganic conductors.[18] A large power factor (PF) $S^2\sigma$ is achieved by large $S$ and $\sigma$, but $S$ usually decreases with increasing $\sigma$.[18,19] Poly(3,4-ethylenedioxythiophene) polystyrenesulfonate (PEDOT: PSS) affords very high PF among organic materials, where the maximum PF ($S^2\sigma$ = 300 $\mu$W K$^{-2}$ m$^{-1}$) is realized by optimal dedoping.[17,18] By using the thermal conductivity of $\kappa$ = 0.24 W K$^{-2}$ m$^{-1}$, this leads to a figure of merit $ZT$ = 0.42. Several small-molecule organic conductors such as (TTF)(TCNQ) and nickel dithiolate complexes have been investigated as thermoelectric materials.[21,22] The PF of single-crystal (TTF)(TCNQ) is 36 $\mu$W K$^{-2}$ m$^{-1}$.[23] In particular, (TTF)(TCNQ) is an important material to show negative thermoelectric power.

Although transport by using field effect and conduction in chemically doped CT salts have been independently investigated, recently carrier number ($n$) dependence of thermoelectric power has been studied by the combined use of field effect and chemical doping.[24,25] $S$ is a decreasing function of $n$, whereas $\sigma$ is an increasing function of $n$, so that the PF makes a maximum at a finite $n$. It should be, however, noted that the charge-carrier density of $10^{21}$ cm$^{-3}$ in a CT complex is by 2 orders of magnitude larger than the field-induced carrier density,[13] where the two-dimensional carrier density of $10^{12}$ cm$^{-2}$ leads to the three-dimensional carrier density of $10^{19}$ cm$^{-3}$.[26] On the other hand, $S$ is inversely proportional to the bandwidth.[23] The bandwidth of $(BTBT)_2PF_6$ has been estimated to be 0.35 eV from the molecular orbital calculation,[13] which is remarkably smaller than 1 eV in TTF conductors. Then, large $S$ is expected, which leads to a large thermoelectric PF together with the high conductivity.

This paper reports a series of newly prepared CT salts $(BTBT)_2XF_6$ containing various octahedral anions, X = As, Sb, and Ta. The experimentally determined bandwidth is as large as 1.4 eV, but the thermoelectric PF is still large (55−88 $\mu$W K$^{-2}$ m$^{-1}$ for the $AsF_6$ salt) owing to the high conductivity. The nature of the insulating state is discussed on the basis of the magnetic and optical properties of $(BTBT)_2PF_6$.

## 2. EXPERIMENTAL SECTION

**2.1. Sample Preparation.** BTBT was prepared according to the previous report.[27] Rodlike black crystals were grown by electrochemical oxidation of BTBT (2−5 mg) in dehydrated dichloromethane using the corresponding tetra-*n*-butylammonium salts as a supporting electrolyte (14−20 mg) under a constant current of 1 $\mu$A at −10 °C for 3 days.

**2.2. X-ray Crystal Structure Analysis.** The diffraction data of the $AsF_6$, $SbF_6$, and $TaF_6$ salts were collected at room temperature by using a Rigaku AFC-7R diffractometer with graphite monochromated Mo K$\alpha$ radiation (0.71069 Å) and a rotating anode generator. The crystal structures were solved by the direct method (SIR2008[28]) and refined by full-matrix least-squares on $F^2$ (SHELXL-97[29]).

**2.3. Band Calculation.** From the results of the X-ray crystal structure analyses, intermolecular overlap integrals were calculated using the highest occupied molecular orbital (HOMO).[30]

**2.4. Resistivity.** Electrical resistivities were measured by the conventional four-probe method using low-frequency AC current. Gold wires (15 $\mu$m $\phi$ diameter) were attached to a crystal using carbon paste. Measurements were carried out parallel to the conducting $c$-axis. The room-temperature conductivity values $\sigma_{av}$ are estimated from the average of three to 12 samples.

**2.5. Thermoelectric Power.** Thermoelectric power was measured by attaching a sample to two copper heat blocks by carbon paste via gold foils. The heat blocks were alternately heated to generate a temperature gradient $\Delta T$ of less than 1 K. The generated voltage $\Delta V$ was recorded, and from the $\Delta V-\Delta T$ linear region, the thermoelectric power was evaluated as $S = \Delta V/\Delta T$.[31] The measurement was carried out parallel to the conducting $c$ axis similarly to the electrical resistivity.

**2.6. Magnetic Properties.** ESR measurements were carried out for single crystals using an X-band spectrometer (JEOL JES-TE100). Owing to the high conductivity, the ESR line shape was a highly asymmetrical Dysonian depending on the field directions.[13] For the easiness of the analysis, a thin needle crystal was placed horizontally, and the magnetic field was applied parallel to the $c$-axis. Then, the observed symmetrical ESR line shape was fitted by a Lorentzian.

**2.7. Optical Properties.** Infrared reflectance spectra were observed by an FT-IR spectrometer, Nicolet Nexus 870 equipped


DOI: 10.1021/jacs.6b01213
J. Am. Chem. Soc. 2016, 138, 3920−3925

with an IR microscope, Spectratech IR-Plan at temperatures between 300 and 4 K. Raman spectra were measured by a micro-Raman spectrogram RENISHAW InVia Reflex in a back scattering geometry using a laser line of 632.8 nm at temperatures between 290 and 4 K.

## 3. RESULTS AND DISCUSSION

**3.1. Crystal Structure.** The crystals are isostructural (Table 1) and belong to a tetragonal space group $P\text{-}42_1c$ (no. 114). The molecular packing of the $AsF_6$ salt is depicted in Figure 1a.

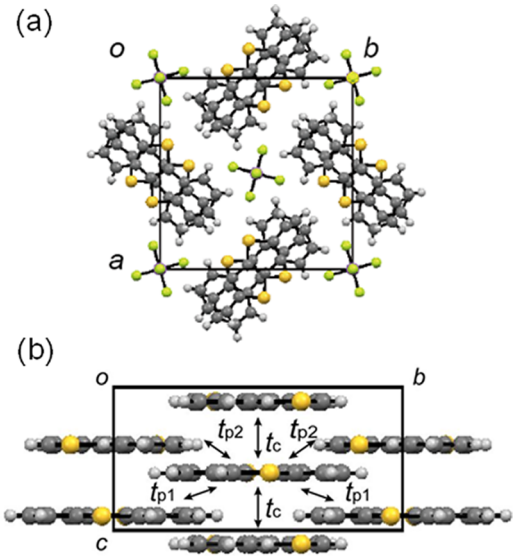


**Figure 1.** (a) Crystal structure of $(BTBT)_2AsF_6$ viewed along the $c$ axis, and (b) donor arrangement viewed along the $a$ axis.

The donor molecules are planar, and form stacks along the $c$ axis. The BTBT molecules are alternately arranged with respect to the sulfur position, but the molecules are related to each other by a $c$-glide plane. Then, the intrastack transfer is uniform, which is designated as $t_c$ in Figure 1b. The molecules in the adjacent stacks are arranged in a windmill manner, where the molecular long axes are perpendicular to each other. With increasing the anion size, the lattice volume increases anisotropically; the $c$ axis does not change largely but the $a$ axis increases predominantly. Then, the interplanar spacing of BTBT, represented by $c/2$, is approximately the same (3.367−3.373 Å, 0.18% change), but the intercolumnar spacing expands depending on the anions (2% change). The interstack transfer integrals are very small (Table 1), and these salts are highly one-dimensional. From the calculated $t_c$ (Table 1), the bandwidth is 0.35 eV, which is practically independent of the anions.

**3.2. Conductivity.** These salts show remarkably high room-temperature conductivity. Table 2 lists the room-temperature conductivity $\sigma$ and the drift mobility $\mu$, calculated from $\sigma = ne\mu$, where $n$ is estimated from the unit cell volume.[13] The conductivity of the $AsF_6$ salt is obviously higher than that of the $PF_6$ salt, but the conductivity successively decreases in the $SbF_6$ and $TaF_6$ salts. It is not possible to directly compare the drift mobility with the field-effect mobility, because the CT salt has a different crystal structure from the neutral crystal. Nonetheless, the estimated large drift mobility is in the same order as the reported field-effect mobility.[1−7]

Figure 2 shows the temperature dependence of the resistivity. These salts exhibit metallic conductivity below room temperature. These salts show large resistivity jumps below 200 K with a large hysteresis between the cooling and heating runs. The temperature dependence just below the jump is nearly flat, but a true insulating state appears below 60 K. The activation energy $E_a$ tends to decrease when the resistivity jump occurs at higher temperature (Table 2). The resistivity jump is, however, suppressed down to low temperatures by coating the crystal with Apiezon N grease (Figure 2b), which applies a pressure of about 0.3 kbar.[13,32] No hysteresis is observed in the Apiezon-covered crystals. The resistivity jump is very sensitive to the pressure, but the insulating state below 60 K is unaffected, in which $E_a$ is generally larger than the noncoated samples.

**Table 2. Room-Temperature Conductivity $\sigma$, Drift Mobility $\mu$, Activation Energy $E_a$, Seebeck Coefficient $S$, and Power Factor $S^2\sigma$ of $(BTBT)_2XF_6$ (X = P, As, Sb, and Ta)[a]**

| | $PF_6$ | $AsF_6$ | $SbF_6$ | $TaF_6$ |
|---|---|---|---|---|
| $\sigma_{av}$ (S cm$^{-1}$) | 1800 | 2600 | 1500 | 640 |
| $\sigma_{max}$ (S cm$^{-1}$) | 2200 | 4100 | 2000 | 1700 |
| $\mu_{av}$ (cm$^2$ V$^{-1}$ s$^{-1}$) | 6.9 | 10.1 | 6.0 | 2.6 |
| $\mu_{max}$ (cm$^2$ V$^{-1}$ s$^{-1}$) | 8.4 | 15.9 | 7.9 | 6.8 |
| $E_a$ (K) | 57 | 43 | 125 | 18 |
| $E_a$ with Apezon (K) | 140 | 93 | 131 | 77 |
| $S_{av}$ ($\mu$V K$^{-1}$) | 15 | 15 | 15 | 15 |
| $S^2\sigma_{av}$ ($\mu$W K$^{-2}$ m$^{-1}$) | 38 | 55 | 38 | 17 |
| $S^2\sigma_{max}$ ($\mu$W K$^{-2}$ m$^{-1}$) | 47 | 88 | 48 | 40 |

[a]The subscripts av and max indicate average and maximum values, respectively.

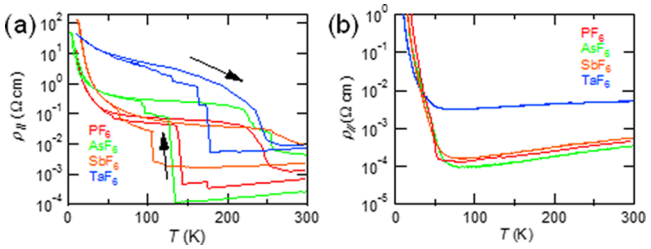


**Figure 2.** Temperature dependence of the resistivity measured along the $c$ axis (a) without and (b) with Apiezon N grease. The results of the $PF_6$ salt are taken from ref 13

**3.3. Thermoelectric Power.** Figure 3 shows the temperature dependence of the thermoelectric power. These salts show a similar value of 15 $\mu$V K$^{-1}$ at room temperature. The positive thermoelectric power indicates hole conduction. The temperature dependence is very similar as well, and the linear

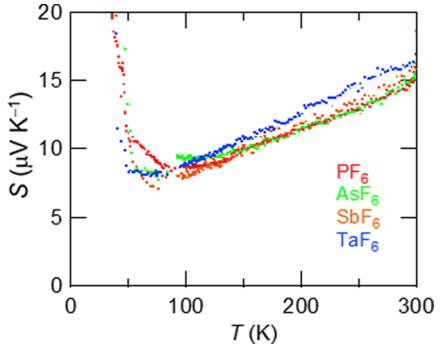


**Figure 3.** Temperature dependence of the Seebeck coefficient of $(BTBT)_2XF_6$.


DOI: 10.1021/jacs.6b01213
J. Am. Chem. Soc. 2016, 138, 3920−3925

dependence down to 60 K is consistent with the metallic conductivity. It is noteworthy that no anomaly is observed associated with the resistance jump. In general, thermoelectric power is insensitive to domain walls and crystal imperfections because the actual current flow is not accompanied. Actually, even the compressed pellet shows a very similar thermoelectric power to the crystal.[21] Assuming the one-dimensional tight-binding energy band, the thermoelectric power $S$ is represented by

$$S = \frac{\pi^2 k_B{}^2 T}{6et} \frac{\cos(\pi\rho/2)}{1 - \cos^2(\pi\rho/2)}$$

where $k_B$ is the Boltzmann constant, and $\rho$ is the charge-transfer degree, which is 0.5 when the energy band is quarter-filled.[23] Then, thermoelectric power is inversely proportional to the bandwidth.[23] From the room-temperature value of 15 $\mu$V K$^{-1}$, the bandwidth is estimated to be 1.4 eV (Supporting Information). This is much larger than the value of 0.35 eV estimated from the molecular orbital calculation. The calculated transfer integral tends to increase with the number of sulfur atoms involved in the molecules due to the large atomic orbital of sulfur.[33] However, it has been experimentally revealed that even molecules such as perylene and fluoranthene, which do not have sulfur atoms, form an energy band as large as 1 eV.[34] The present result is an ambiguous evidence that BTBT forms an energy band as large as 1 eV similarly to TTF conductors. Such a large bandwidth is potentially related to the high mobility of the BTBT transistors, where the calculation affords similarly small transfer integrals.[33]

The power factor $S^2\sigma$ is as large as 55 $\mu$W K$^{-2}$ m$^{-1}$ in the $AsF_6$ salt, and the maximum value is 88 $\mu$W K$^{-2}$ m$^{-1}$ (Table 2). Although the power factor in the optimally doped PEDOT:PSS is as large as 300 $\mu$W K$^{-2}$ m$^{-1}$, the ordinary PEDOT:PSS exhibits about 40 $\mu$W K$^{-2}$ m$^{-1}$.[2] The observed $S$ is not as large as expected from the molecular orbital calculation, but the resulting PF is comparatively large among organic thermoelectric materials.

**3.4. Magnetic Properties.** On account of the high conductivity, the ESR signal shows a highly asymmetrical Dysonian shape depending on the crystal size.[13] Since this is due to the skin effect on the crystal surface, only sufficiently thick crystals show the Dysonian shape. Then, we have selected thin crystals and analyzed the results assuming the symmetrical Lorentzian model. Figure 4 shows the temperature dependence of the normalized spin susceptibility ($\chi$), and the peak-to-peak line width ($\Delta H_{pp}$). The susceptibility decreases gradually, but does not go down to zero (Figure 4a). Thus, the low-temperature insulating state is considered to be essentially paramagnetic. The $g$ values are 2.002 and constant down to low temperatures (Supporting Information). The line width increases when the anion element becomes heavy (Figure 4b). At low temperatures, the line width increases gradually, but the resistance jump does not afford any influence. Below 30 K, the line width decreases slightly. Accordingly, the possibility of magnetic order is excluded as an origin of the insulating state.

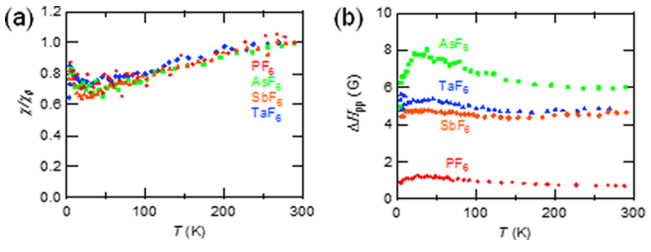


**Figure 4.** Temperature dependence of (a) the normalized spin susceptibility and (b) the peak-to-peak line width.

**3.5. Optical Properties.** To investigate the nature of the low-temperature ground state, Raman and infrared (IR) spectra are measured for $(BTBT)_2PF_6$. Figure 5 shows the temperature dependence of the reflectance spectra for $E//c$. The reflectance exhibits a Drude-like increase below 8000 cm$^{-1}$, but decreases again below 2000 cm$^{-1}$. This suggests the existence of a small energy gap even at room temperature. Then, the spectrum is analyzed by assuming the Drude–Lorentz model (Supporting Information), and the plasma frequency is estimated to be $\omega_P$ = 11500 cm$^{-1}$ at room temperature. Assuming the one-dimensional tight-binding approximation, this leads to the bandwidth of $4t_c$ = 1.35 eV.[35] This value is in good agreement with the estimation from the thermoelectric power.

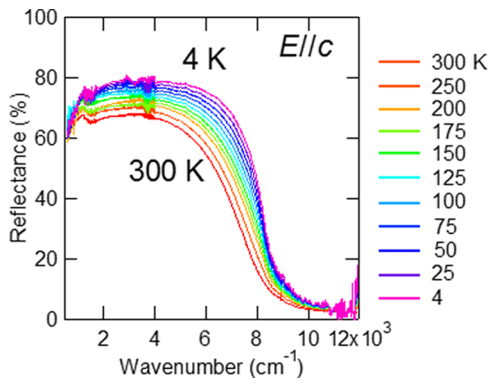


**Figure 5.** Reflectance spectra of $(BTBT)_2PF_6$ ($E//c$) at various temperatures.

Figure 6a shows the optical conductivity spectra calculated from the IR reflectance using the Kramers–Kronig relation.

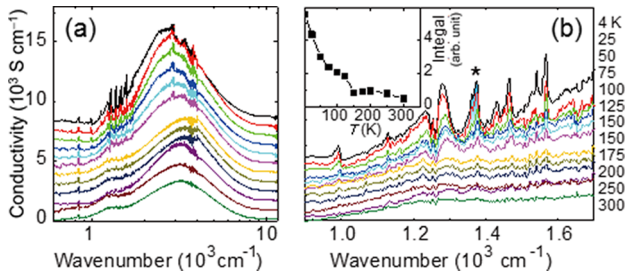


**Figure 6.** (a) Conductivity spectra of $(BTBT)_2PF_6$ ($E//c$) at various temperatures. The vertical scale is offset for clarity. (b) Magnified plot of the mid-IR region. The inset shows the temperature dependence of the integrated intensity for the 1380 cm$^{-1}$ peak (*).

The spectra show a broad band around 3200 cm$^{-1}$, indicating charge localization even at room temperature. The growing conductivity peak indicates development of an energy gap at low temperatures.

It is noteworthy that a number of peaks in the mid-IR range are enhanced at low temperatures (Figure 6b). The asymmetric shape of the peaks are characteristic of the electron-molecular vibration (e-mv) coupling,[36] thus the signals are ascribed to $a_g$ type of molecular vibrations. Although the X-ray structure indicates uniform stacking, the activation of the e-mv bands


DOI: 10.1021/jacs.6b01213
J. Am. Chem. Soc. 2016, 138, 3920–3925

demonstrates the modulated stacking. The temperature dependence of the integrated intensity is plotted in the inset of Figure 6b for the 1380 $cm^{-1}$ peak ($\nu_9$). This vibronic peak exists even at room temperature, and the peak intensity remarkably increases below 150 K at which the resistivity jump is observed. Then, the modulation, presumably stemming from the one-dimensional instability, is closely related to the insulating state.

Figure 7a shows the Raman spectra at various temperatures. The Raman peaks and the IR e-mv bands (Figure 7b) are

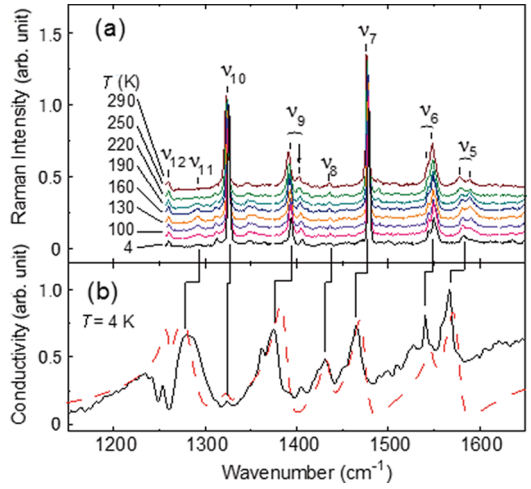


**Figure 7.** (a) Raman spectra of $(BTBT)_2PF_6$ at various temperatures. Peak assignments are done on the basis of the density functional calculation. (b) Optical conductivity spectrum in the insulating phase at 4 K (solid curve) and the calculated spectrum based on a dimeric cluster model (broken curve). Correspondence between the Raman and vibronic IR peaks is indicated by the cranked lines.

assigned on the basis of the density functional calculation (Supporting Information). A numerical fit to the IR spectrum using a symmetric dimer model (Supporting Information) reproduces the asymmetric shape and the observed frequencies satisfactorily (broken curve in Figure 7b).[37] This indicates that the modulation, which accounts for the insulator transition, is essentially ascribed to the dimerization.

It should be mentioned that several Raman peaks appear as a doublet (for example, $\nu_5$, $\nu_6$, and $\nu_9$). Such peak splitting recalls tetramerization due to the $2k_F$ charge-density-wave (Peierls) state that is observed in quarter-filled systems like $(Perylene)_2PF_6$ and $(Fluoranthene)_2PF_6$.[34] However, such modulation is excluded owing to the observed paramagnetic susceptibility (Figure 4a). As another candidate, one may assume symmetry reduction due to charge ordering.[38] The splitting is, however, not compatible with the ionicity dependence of the different modes (Supporting Information). In addition, the IR spectrum is successfully fitted by the dimer model. Then, we conclude that the Raman doublets are derived from a factor group splitting. The observed paramagnetic insulator phase is preferably ascribed to a $4k_F$ charge-density-wave state. Here, the donor stack is slightly dimerized owing to the alternating $t_c$, whereas the lattice parameter $c$ is unchanged because of the original two-molecule repeating unit.[13] Each dimer has one unpaired spin, which is localized due to the Coulomb repulsion, and forms a Mott insulating state. The $4k_F$ instability exists even at room temperature, then the molecules dimerize gradually and somewhat irreversibly at low temperatures.

## 4. CONCLUSIONS

We have investigated the physical properties of highly conducting one-dimensional organic metals, $(BTBT)_2XF_6$ (X = P, As, Sb, and Ta). From the thermoelectric power and the reflectance spectrum, the bandwidth is determined to be as large as 1.4 eV. This is the evidence that the BTBT molecules, which involve only two sulfur atoms, mediate large intermolecular interaction. Owing to the high conductivity, the $AsF_6$ salt shows a large power factor of 55−88 $\mu W\ K^{-2}\ m^{-1}$ among organic thermoelectric materials. From the paramagnetic susceptibility and the spectroscopic investigations, the insulating state is attributed to the $4k_F$ charge-density waves. Accordingly, BTBT realizes a large bandwidth, but the on-site Coulomb repulsion is still important, so BTBT resembles TTF family donors rather than TCNQ and aromatic hydrocarbons such as perylene. By the use of not only field-effect transistors but also chemical doping, we can extend new possibilities of BTBT-based materials.

## ■ ASSOCIATED CONTENT

### Supporting Information

The Supporting Information is available free of charge on the ACS Publications website at DOI: 10.1021/jacs.6b01213.

Calculated energy bands, estimation of drift mobility, Arrhenius plots, estimation of the bandwidth from the Seebeck coefficient, ESR measurements, and analyses of the IR and Raman spectra. (PDF)

Crystallographic data in CIF format for $C_{28}H_{16}AsF_6S_4$ (CIF)

Crystallographic data in CIF format for $C_{28}H_{16}F_6S_4Sb$ (CIF)

Crystallographic data in CIF format for $C_{28}H_{16}F_6S_4Ta$ (CIF)

## ■ AUTHOR INFORMATION


### Corresponding Authors

*kadoya.t@sci.u-hyogo.ac.jp

*yamamoto@dap.ous.ac.jp

*mori.t.ae@m.titech.ac.jp

### Present Addresses

⊥T.K.: Graduate School of Material Science, University of Hyogo, 3-2-1 Koto, Kamigori-cho, Ako-gun, Hyogo 678-1297, Japan.

#T.H.: Institute for Solid State Physics, The University of Tokyo, Kashiwa, Chiba 277-8581, Japan.


### Notes

The authors declare no competing financial interest.

## ■ ACKNOWLEDGMENTS

This work was partly supported by a Grant-in Aid for Scientific Research (B) (No. 23350061) from the Ministry of Education, Culture, Sports, Science, and Technology of Japan.

## ■ REFERENCES


(1) Takimiya, K.; Ebata, H.; Sakamoto, K.; Izawa, T.; Otsubo, T.; Kunugi, Y. *J. Am. Chem. Soc.* **2006**, *128*, 12604−12605.

(2) Ebata, H.; Izawa, T.; Miyazaki, E.; Takimiya, K.; Ikeda, M.; Kuwabara, H.; Yui, T. *J. Am. Chem. Soc.* **2007**, *129*, 15732−15733.

(3) Izawa, T.; Miyazawa, E.; Takimiya, K. *Adv. Mater.* **2008**, *20*, 3388−3392.

(4) Takimiya, K.; Shinamura, S.; Osaka, I.; Miyazaki, E. *Adv. Mater.* **2011**, *23*, 4347−4370.




DOI: 10.1021/jacs.6b01213
J. Am. Chem. Soc. 2016, 138, 3920−3925

(5) Minemawari, H.; Toshikazu, Y.; Matui, H.; Tsutsumi, J.; Haas, S.; Chiba, R.; Kumai, R.; Hasegawa, T. *Nature* **2011**, *475*, 364−367.
(6) Yuan, Y.; Giri, G.; Ayzner, A. L.; Zoombelt, A. P.; Mannsfeld, S. C. B.; Chen, J.; Nordlund, D.; Toney, M. F.; Huang, J.; Bao, Z. *Nat. Commun.* **2014**, *5*, 3005−3013.
(7) Cho, J.; Higashino, T.; Mori, T. *Appl. Phys. Lett.* **2015**, *106*, 193303−193306.
(8) Coleman, L. B.; Cohen, M. J.; Sandman, D. J.; Yamagishi, F. G.; Garito, A. F.; Heeger, A. J. *Solid State Commun.* **1973**, *12*, 1125−1132.
(9) (a) Di, C.; Yu, G.; Liu, Y.; Xu, X.; Wei, D.; Song, Y.; Sun, Y.; Wang, Y.; Zhu, D.; Liu, J.; Liu, X.; Wu, D. *J. Am. Chem. Soc.* **2006**, *128*, 16418−16419. (b) Di, C.; Yu, G.; Liu, Y.; Guo, Y.; Wang, Y.; Wu, W.; Zhu, D. *Adv. Mater.* **2008**, *20*, 1286−1290.
(10) (a) Shibata, K.; Wada, H.; Ishikawa, K.; Takezoe, H.; Mori, T. *Appl. Phys. Lett.* **2007**, *90*, 193509−193511. (b) Pfattner, R.; Mas-Torrent, M.; Moreno, C.; Puigdollers, J.; Alcubilla, R.; Bilotti, I.; Venuti, E.; Brillante, A.; Laukhin, V.; Veciana, J.; Rovira, C. *J. Mater. Chem.* **2012**, *22*, 16011−16016.
(11) (a) Tamura, S.; Kadoya, T.; Kawamoto, T.; Mori, T. *Appl. Phys. Lett.* **2013**, *102*, 063305−063308. (b) Tamura, S.; Kadoya, T.; Mori, T. *Appl. Phys. Lett.* **2014**, *105*, 023301−023304. (c) Kadoya, T.; Tamura, S.; Mori, T. *J. Phys. Chem. C* **2014**, *118*, 23139−23146.
(12) (a) Mendez, H.; Heimel, G.; Opitz, A.; Sauer, K.; Barkowski, P.; Oehzelt, M.; Soeda, J.; Okamoto, T.; Takeya, J.; Arlin, J.-B.; Balandier, J.-Y.; Geerts, Y.; Koch, N.; Salzmann, I. *Angew. Chem., Int. Ed.* **2013**, *52*, 7751−7755. (b) Tsutsumi, J.; Matsuoka, S.; Inoue, S.; Minemawari, H.; Yamada, T.; Hasegawa, T. *J. Mater. Chem. C* **2015**, *3*, 1976−1981. (c) Shibata, Y.; Tsutsumi, J.; Matsuoka, S.; Matsubara, K.; Yoshida, Y.; Chikamatsu, M.; Hasegawa, T. *Appl. Phys. Lett.* **2015**, *106*, 143303−143306.
(13) Kadoya, T.; Ashizawa, M.; Higashino, T.; Kawamoto, T.; Kumeta, S.; Matsumoto, H.; Mori, T. *Phys. Chem. Chem. Phys.* **2013**, *15*, 17818−17822.
(14) Seo, H.; Hotta, C.; Fukuyama, H. *Chem. Rev.* **2004**, *104*, 5005−5036.
(15) Bubnova, O.; Crispin, X. *Energy Environ. Sci.* **2012**, *5*, 9345−9362.
(16) Zhang, Q.; Sun, Y.; Xu, W.; Zhu, D. *Energy Environ. Sci.* **2012**, *5*, 9639−9644.
(17) Kim, G.-H.; Shao, L.; Zhang, K.; Pipe, K. P. *Nat. Mater.* **2013**, *12*, 719−723.
(18) Bubnova, O.; Khan, Z. U.; Malti, A.; Braun, S.; Fahlman, M.; Berggren, M.; Crispin, X. *Nat. Mater.* **2011**, *10*, 429−433.
(19) Zhang, Q.; Sun, Y.; Xu, W.; Zhu, D. *Adv. Mater.* **2014**, *26*, 6829−6851.
(20) (a) Bubnova, O.; Berggren, M.; Crispin, X. *J. Am. Chem. Soc.* **2012**, *134*, 16456−16459. (b) Hiroshige, Y.; Ookawa, M.; Toshima, N. *Synth. Met.* **2007**, *157*, 467−474. (c) Massonnet, N.; Carella, A.; Jaudouin, O.; Rannou, P.; Laval, G.; Celle, C.; Simonato, J.-P. *J. Mater. Chem. C* **2014**, *2*, 1278−1283. (d) Kemp, N. T.; Kaiser, A. B.; Liu, C. J.; Chapman, B.; Mercier, O.; Carr, A. M.; Trodahl, H. J.; Buckley, R. G.; Partridge, A. C.; Lee, J. Y.; Kim, C. Y.; Bartl, A.; Dunsch, L.; Smith, W. T.; Shapiro, J. S. *J. Polym. Sci., Part B: Polym. Phys.* **1999**, *37*, 953−960. (e) Aich, R. B.; Blouin, N.; Bouchard, A.; Leclerc, M. *Chem. Mater.* **2009**, *21*, 751−757. (f) Tamayo, E.; Hayashi, K.; Shinano, T.; Miyazaki, Y.; Kajitani, T. *Appl. Surf. Sci.* **2010**, *256*, 4554−4558. (g) Yoshino, H.; Papavassiliou, G. C.; Murata, K. *J. Therm. Anal. Calorim.* **2008**, *92*, 457−460.
(21) Wusten, J.; Potje-Kamloth, K. *J. Phys. D: Appl. Phys.* **2008**, *41*, 135113−135120.
(22) Sun, Y.; Sheng, P.; Di, C.; Jiao, F.; Xu, W.; Qiu, D.; Zhu, D. *Adv. Mater.* **2012**, *24*, 932−937.
(23) Chaikin, P. M.; Greene, R. L.; Etemad, S.; Engler, E. *Phys. Rev. B* **1976**, *13*, 1627−1632.
(24) Zhang, Q.; Zang, Y.; Huang, D.; Di, C.; Gao, X.; Sirringhaus, H.; Zhu, D. *Adv. Funct. Mater.* **2015**, *25*, 3004−3012.
(25) Pernstich, K. P.; Rossner, B.; Batlogg, B. *Nat. Mater.* **2008**, *7*, 321−325.
(26) (a) Akiyama, Y.; Mori, T. *AIP Adv.* **2014**, *4*, 017126. (b) Cho, J.; Akiyama, Y.; Kakinuma, T.; Mori, T. *AIP Adv.* **2013**, *3*, 102131−102144.
(27) Li, Y.; Nie, C.; Wang, H.; Li, H.; Verpoort, F.; Duan, C. *Eur. J. Org. Chem.* **2011**, *36*, 7331−7338.
(28) Burla, M. C.; Caliandro, R.; Camalli, M.; Carrozzini, B.; Cascarano, G. L.; de Caro, L.; Giacovazzo, C.; Polidori, G.; Siliqi, D.; Spagna, R. *J. Appl. Crystallogr.* **2007**, *40*, 609−613.
(29) Sheldrick, G. M. *Acta Crystallogr., Sect. A: Found. Crystallogr.* **2008**, *64*, 112−122.
(30) (a) Dewar, M. J. S.; Zoebisch, E. G.; Healy, E. F.; Stewart, J. J. P. *J. Am. Chem. Soc.* **1985**, *107*, 3902−3909. (b) Mori, T.; Kobayashi, A.; Sasaki, Y.; Kobayashi, H.; Saito, G.; Inokuchi, H. *Bull. Chem. Soc. Jpn.* **1984**, *57*, 627−633.
(31) Chaikin, P. M.; Kwark, J. F. *Rev. Sci. Instrum.* **1975**, *46*, 218−220.
(32) Wang, H. H.; Kini, A. M.; Montgomery, L. K.; Geiser, U.; Carlson, K. D.; Williams, J. M.; Thompson, J. E.; Watkins, D. M.; Kwok, W. K.; Welp, U.; Vandervoort, K. G. *Chem. Mater.* **1990**, *2*, 482−484.
(33) Kojima, H.; Mori, T. *Bull. Chem. Soc. Jpn.* **2011**, *84*, 1049−1056.
(34) (a) Wilckens, R.; Geserich, H. P.; Ruppel, W.; Koch, P.; Schweitzer, D.; Keller, H. J. *Solid State Commun.* **1982**, *41*, 615−618. (b) Geserich, H. P.; Koch, B.; Ruppel, W.; Wilckens, R.; Schweitzer, D.; Enkelmann, V.; Wegner, G.; Wieners, G.; Keller, H. J. *J. Phys. Colloq.* **1983**, *44*, C3-1461−1464.
(35) Kawamoto, T.; Ashizawa, M.; Aragaki, M.; Mori, T.; Yamamoto, T.; Tajima, H.; Kitagawa, H.; Mitani, T.; Misaki, Y.; Tanaka, K. *Phys. Rev. B: Condens. Matter Mater. Phys.* **1999**, *60*, 4635−4645.
(36) Rice, M. J.; Lipari, N. O. *Phys. Rev. Lett.* **1977**, *38*, 437−439.
(37) Rice, M. J. *Solid State Commun.* **1979**, *31*, 93−98.
(38) (a) Yamamoto, K.; Yakushi, K.; Miyagawa, K.; Kanoda, K.; Kawamoto, A. *Phys. Rev. B* **2004**, *69*, 085114−085124. (b) Tajima, H.; Kyoden, S.; Mori, H.; Tanaka, S. *Phys. Rev. B: Condens. Matter Mater. Phys.* **2000**, *62*, 9378−9386.


DOI: 10.1021/jacs.6b01213
*J. Am. Chem. Soc.* 2016, 138, 3920−3925